Noname manuscript No.
(will be inserted by the editor)

An open electromagnetic tracking framework applied to targeted liver tumour ablation

Stephen Hinds · Herman Alexander Jaeger · Richard Burke · Brodie O'Sullivan · Joseph Keane · Fabian Trauzettel · Bruno Marques · Stéphane Cotin · Brian Bird · Håkon Olav Leira · Erlend Fagertun Hofstad · Ole Vegard Solberg · Thomas Langø · Pádraig Cantillon-Murphy

Received: date / Accepted: date

Abstract *Purpose* Electromagnetic tracking is a core platform technology in the navigation and visualisation of image-guided procedures. The technology provides high tracking accuracy in non-line-of-sight environments, allowing instrument navigation in locations where optical tracking is not feasible. EMT can be beneficial in applications such as percutaneous radiofrequency ablation for the treatment of hepatic lesions where the needle tip may be obscured due to difficult liver environments (e.g subcutaneous fat or ablation artefacts). Advances in the field of EMT include novel methods of improving tracking system accuracy, precision and error compensation capabilities, though such system-level improvements cannot be readily incorporated in current therapy applications due to the 'blackbox' nature of commercial tracking solving algorithms. *Methods* This paper defines a software framework to allow novel EMT designs and improvements become part of the global design process for image-guided interventions. An exemplary framework is implemented in the Python programming language and demonstrated with the open-source Anser EMT system. The framework is applied in the preclinical setting though targeted liver ablation therapy on an animal model. *Results* The developed framework was tested with the Anser EMT electromagnetic tracking

Supported by Science Foundation Ireland technical innovation and development award number 17/TIDA/4897.

S.Hinds, H.Jaeger, R.Burke, B.O'Sullivan, F.Trauzettel, P.Cantillon-Murphy
University College Cork, Ireland
E-mail: h.jaeger@umail.ucc.ie

B.Marques, S.Cotin
INRIA, Strasbourg, France

B.Bird
Bon Secours Hospital, Cork, Ireland

J.Keane
Sunbeam Veterinary Hospital, Cork, Ireland

H.O.Leira, E.F.Hofstad, O.V.Solberg, T.Langø
SINTEF, Trondheim, Norway

platform. Liver tumour targeting was performed using the tracking framework with the CustusX navigation platform using commercially available electromagnetically tracked needles. Ablation of two tumours was performed with a commercially available ablation system. Necropsy of the tumours indicated ablations within 5 mm of the tumours. *Conclusions* An open source framework for electromagnetic tracking was presented and effectively demonstrated in the pre-clinical setting. We believe that this framework provides a structure for future advancement in EMT system in and customised instrument design.

Keywords Image-guided intervention · Electromagnetic tracking · Surgical navigation

1 Introduction

The development of new image guided therapies relies heavily on intelligently combining data from multiple hardware devices. New techniques combining ultrasound and electromagnetic tracking (EMT) [1,2] are among techniques which combine multiple data sources to enhance the safety and accuracy of procedures. Progress in these areas is made possible by the standardised open protocols [3,4] that govern how hardware and software should interact with one another. Fig. 1 shows the generalised design flow of many image guided interventions (IGI). IGI applications interact with hardware through vendor authored application programming interfaces (APIs) or interface toolkits such as PLUS and IGSTK[5]. Open-source software is becoming increasing popular among research groups as it enables a common infrastructure to be shared and standardised. However, IGI application development typically falls short of incorporating custom innovations in tracking hardware. Electromagnetic tracking systems in particular are very much considered 'blackboxes' from the perspective of IGI research, which can limit innovation in tracked instrument design for advanced procedures and therapies.

Percutaneous needle-based procedures such as radiofrequency ablation (RFA) and electrochemotherapy are becoming more prevalent in the treatment of hepatocellular carcinoma [6,7] . Ultrasound is a common imaging modality used in RFA with numerous studies have demonstrating its effectiveness in treating shallow or superficial hepatic lesions [8]. For smaller tumours, fusion imaging or contrast-enhanced US is often necessary [9]. Ultrasound-guided RFA in conjunction with electromagnetic tracking may improve instrument visualisation by providing out-of-plane electrode tracking and identifying the needle tip in difficult liver environments (e.g subcutaneous fat or ablation artefacts as well as needle tip obstruction [10]).

This paper outlines a software framework to encourage integration of new electromagnetic tracking hardware into the current IGI design flow. The resulting framework was implemented in the Python programming language and applied to the open-source Anser EMT system [11] shown in Fig. 2. Preliminary cross-platform functionality of the framework is demonstrated with important performance metrics reported. The effectiveness of an open approach is demonstrated in the pre-clinical setting through the targeted radiofrequency ablation of model liver tumours. Commercially available tracked needles are calibrated for use with the Anser system and used to guide the radiofrequency ablation probes to multiple tumour sites in a swine model using an open-source visualisation framework, CustusX [12].

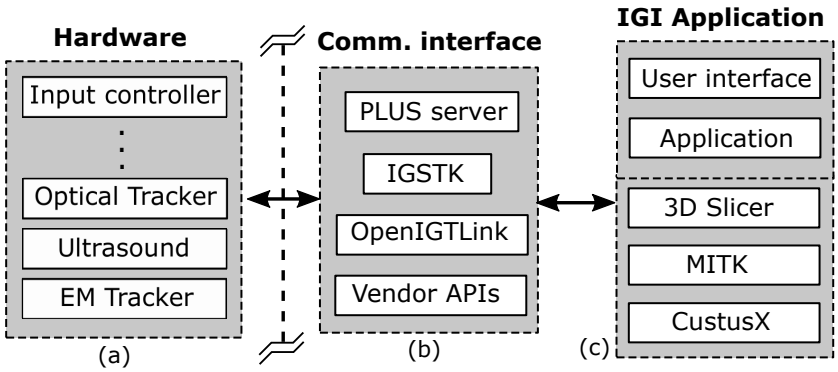

Fig. 1 A standard approach for developing cross-platform IGI applications. (a) Proprietary hardware is interfaced using an API or open communications interface (b). (c) Guided therapy applications use this interface to ensure cross-platform compatibility.

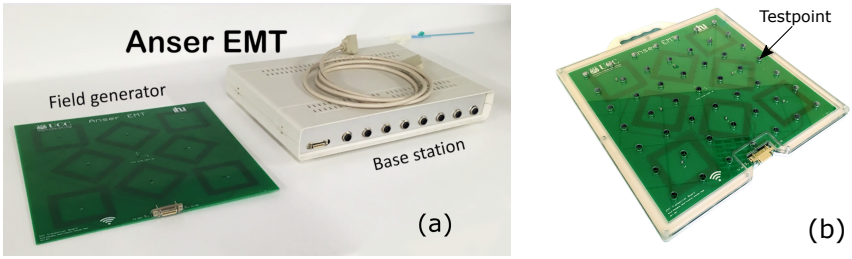

Fig. 2 (a) The Anser EMT system v1.0 consisting of a field generator and base station (b) Field generator enclosure with precision machined holes for tracking sensor calibration.

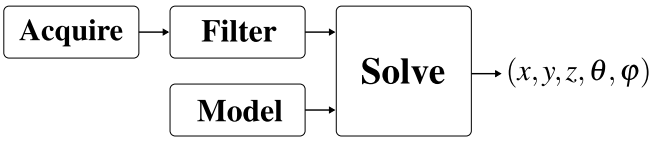

Fig. 3 The basic components which comprise all electromagnetic tracking systems are shown. The 5 degree-of-freedom sensor coordinate $[x, y, z, \theta, \varphi]$ is the most basic case for a symmetrical sensor coil, where θ and φ correspond to yaw and pitch angles respectively.

2 Framework Design

Electromagnetic tracking systems are complex electronic systems that incorporate advanced analog circuit design, signal processing and optimisation techniques. While the precise topology of such systems will vary depending on the core design and manufacturer, all EMT systems can be distinguished by four common processing steps outlined in Fig. 3: *acquisition*, *filtering*, *modelling*, and *solving*. Each of these processing steps can be treated as a discrete, independent stage in the tracking system software pipeline. The designed framework is structured according to these stages.

2.1 Data acquisition

Data acquisition is the process by which physical signals are digitised into forms suitable for computation and is a fundamental step in any measurement system. In the case of EMT systems, the signals being measured are typically electric voltages. Such signals are induced on a tracking sensor coil when it is placed in the tracking volume of an EMT system. Acquisition hardware in the form of an analogue-to-digital converter (ADC) converts the electrical signal into a digital data stream by sampling at fixed periodic intervals. Manufacturers of acquisition systems include National Instruments (Austin, TX, U.S.A.) and Measurement Computing Corp. (Norton, MA, U.S.A). Commercially available electromagnetic tracking systems implement proprietary acquisition schemes that are inaccessible to the user.

2.2 Filtering & extraction

The sampled sensor signal contains all the necessary physical information required to resolve the sensor's position in space. EMT systems typically operate using multiple transmitters operating at distinct frequencies, thus the sampled sensor signal is a linear sum of the individual frequency components generated by each transmitting coil, as well as noise from the surrounding environment. The filter extracts the signal content of interest, from which the position of the sensor can be resolved. A combination of digital filtering and Fourier methods are typically employed. Common signal extraction methods include discrete fourier transform (DFT) methods [13], lock-in amplification [14], Goertzel's algorithm [15] and direct amplitude detection [16].

2.3 Magnetic model

An accurate model of the tracking system's generated magnetic field is a necessary component in all magnetic tracking system designs. The purpose of the model is to predict the physical interaction between the system's magnetic field generator and tracking sensors. Field generator models are typically defined as analytical expressions which define the spacial distribution of magnetic fields in the volume around the field generator. The sensor is model is based on its design, geometry and from which its electrical response can be predicted in the presence of the modelled magnetic field.

Magnetic field generators generally consist of an array of coil which can take on varying sizes and geometries depending on the application. Designs include large circular coils [17], square circuit board coils [11] and small cylindrical elements [18]. Each constituent generating coil in the array produces an alternating magnetic field at a known distinct frequency. In generally, the magnetic field strength or *flux density* due to single coil can be represented by a vector function relating the amplitude of the generated magnetic field in space, $\mathbf{B}$:

$$\mathbf{B}(\mathbf{r}) = [B_x, B_y, B_z] \tag{1}$$

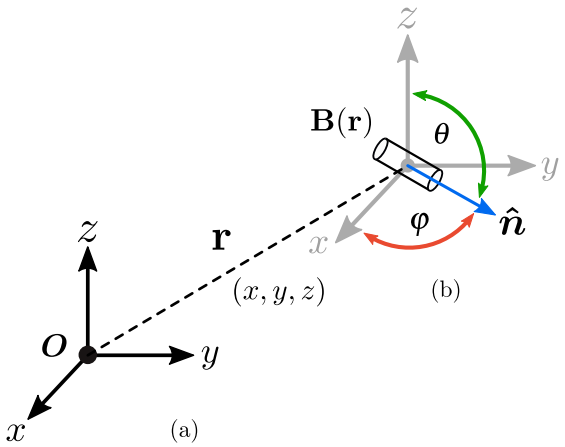

Fig. 4 The basic components which comprise all electromagnetic tracking systems are shown. The 5 degree-of-freedom sensor coordinate $[x, y, z, \theta, \varphi]$ is the most basic case for a symmetrical sensor coil, where θ and φ correspond to yaw and pitch angles respectively.

where B_x, B_y and B_z are orthogonal magnetic flux density vector components, and $\mathbf{r} = (x, y, z)$ is the Cartesian coordinate at which the field is measured with respect to some global origin $\boldsymbol{O}$, shown in Fig. 4(a).

A magnetic tracking sensor is a device which detects the generated magnetic field and produces an output signal whose amplitude is related to its position and orientation with respect to the field generator. In the case of a generalised, solenoidal five degree-of-freedom (5-DoF) magnetic sensor, the sensed magnetic flux density occurs along the axis of the sensor as shown in Fig.4(b). The resulting flux magnetic flux in the sensor, Φ, is given by:

$$\Phi(\mathbf{r}, \theta, \varphi) = K \cdot \mathbf{B}(\mathbf{r}) \cdot \hat{\mathbf{n}}\,(\theta, \varphi) \tag{2}$$

where $\mathbf{B}(\mathbf{r})$ is the magnetic flux density due to a single field generating coil at the point $\mathbf{r}$, K is a geometry dependant constant representing the sensitivity of the sensor and $\hat{\mathbf{n}}$ is a vector representing the orientation of the sensor as a function of its *elevation* and *azimuthal* angles (θ, φ) with respect to the origin as shown in Fig. 4. The variables $\mathbf{r}$, θ and ϕ constitute the five degrees of freedom in which the motion of the sensor may be tracked. Combining these variables into a single vector we define the position and orientation vector of the sensor, $\mathbf{p}$:

$$\mathbf{p} = (x, y, z, \theta, \varphi) \tag{3}$$

2.4 Position solver

Magnetic tracking systems resolve sensor positions by fitting the acquired sensor data to a magnetic model of the system. The *cost* is typically defined as the difference between the physical sensor voltage measurement, V_s, and the modelled sensor voltage signal given by the rate-of-change of the magnetic flux in (2), $\dot{\Phi}_m(\mathbf{p})$, at some location $\mathbf{p}$:

$$Cost = \left(V_s - \dot{\Phi}_m(\mathbf{p})\right)^2 \tag{4}$$

The value of **p** which minimises *Cost*, in a global sense, is defined the sensor position and orientation. In the case of a 5-DoF sensor tracking system, a fully-defined system requires that there exist at least five independent sensor measurements. This can be readily achieved using multiple field generating coils at distinct frequencies. In practice, a minimum of eight frequencies is required to yield accurate and consistent tracking performance [19,20]. For a tracking system consisting of n distinct fields generating coils, the sum-of-squares cost function F is defined as:

$$F(\mathbf{p}) = \sum_{i=1}^{n} \left(V_s^i - \dot{\Phi}_m^i(\mathbf{p}) \right)^2 \tag{5}$$

where i is the index of the field generating coil under consideration. The minimisation process can be performed in real-time using well-known optimisation techniques [21].

3 Framework implementation

The proposed EMT framework is composed of four Python modules representing each of the signal processing steps shown in Fig. 1. An expansion of this design showing the data-flow between modules is shown in Fig. 5. The framework is divided into four modules labelled (i) to (iv). Analog signals from the EMT sensing electronics are acquired through a data acquisition module *daq.py*. This module provides facilities to abstract the acquisition hardware's specific API into a standard interface. The acquired digital samples are fed into the filter module *filter.py* where the frequency components of interest are conditioned and extracted from the digital waveform. The filter module allows easy configuration of filter parameters while providing routines for efficient matrix multiplications required during filtering operations. The extracted signal information is then fed to the solver module *solver.py*. Simultaneously the magnetic model of the system *model.py* is compared with the extracted signal data to minimise the system cost function. The solver module provides access to the tolerance and parameter settings for the minimisation process. The resulting sensor coordinates from the solver can be streamed to the user application using OpenIGTLink [4].
The proposed framework was applied to the Anser EMT project [11]. The original open-source codebase, which was originally implemented in Matlab, was fully converted to Python in order to conform with the framework. The PyDAQmx driver [22] was used to provide a cross-platform interface with the NI-DAQmx driver acquisition system (National Instruments, Austin, Texas). Filtering and solving operations were performed using NumPy and SciPy libraries [23]. OpenIGTLink connectivity was achieved using PyIGTLink [24].

A cross-platform graphical user interface (GUI) was developed to provide an intuitive user experience and simplified access to core tracking system function in the clinical setting. The interface was written using the Qt widget toolkit (The Qt Company, Oslo, Norway) and builds upon the tracking framework to provide an interface specific to the Anser tracking system [11]. The interface is shown in Fig. 6 and consists of tabbed windows which provide interfaces for the calibration, tracking and visualisation of tracked instruments. The GUI also features OpenIGTLink compatibly and is capable of transmitting sensor position data to other visualisation

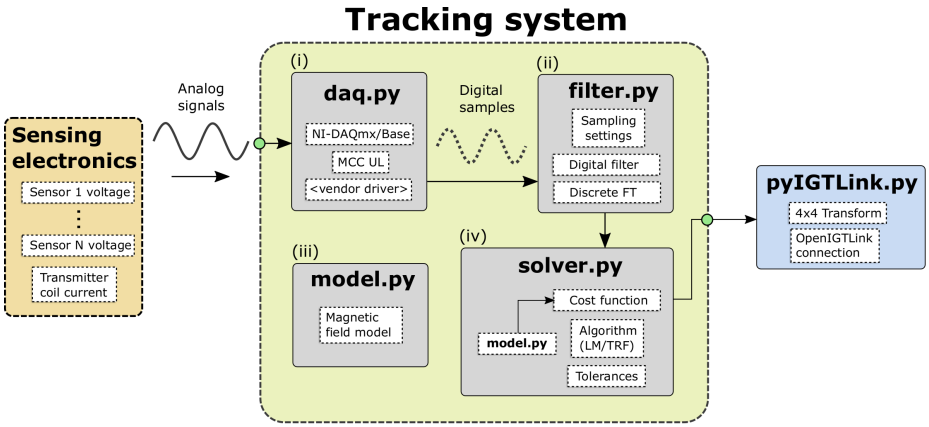

Fig. 5 (i) Analogue signals are sampled by the data acquisition module. (ii) The samples are filtered in software with relevant frequency components extracted. (iii)-(iv) A cost function utilises the component magnitudes to yield a position vector which can be transmitted using OpenIGTLink as a 4x4 transformation matrix.

packages such as 3D Slicer, MITK and CustusX. Implementations of the framework and graphcial user interface are available on (https://openemt.org).

3.1 Framework benchmark

EMT framework's performance and accuracy were tested relative to the original Windows-only Matlab implementation. Testing of the framework was performed on three operating systems: Windows 10, MacOS 10.13 and Cent-OS 7.0 Linux. All reported metrics result from tests performed on a laptop PC configured with an Intel i7 4810HQ 3.5GHz CPU and 16GB of RAM, utilising both a Windows 10 and CentOS 7.0 installation. Compatibility with the MacOS 10.13 operating system was confirmed using a separate machine, but comparative results were not possible due to significant differences in the laptop hardware configuration. The user-adjustable sampling frequency of the acquisition system was set at 100kHz for all experiments.

Performance testing measured the framework's ability to stream position measurements as quickly as possible with minimal latency over an OpenIGTLink connection to CustusX and 3DSlicer. Acquisition latency, maximum update frequency (with both a stationary and moving sensor) were recorded for multiple acquisition frame sizes shown in Tables 1 and 2. An acquisition frame constitutes the number of samples gathered by the acquisition system per single resolved position. A finite acquisition time for each frame puts a limit on the minimum latency figure. Static refers to a slow moving sensor speeds of <5cm per second while 'Dynamic' refers to speeds >50cm per second.

Accuracy testing consisted of comparing errors between sensor positions obtained from a 7x7 plane test x-y grid providing a total of 49 points. 150 position acquisitions at a height of $z = 70$mm from the transmitter board (Fig. 2 (b)) were recorded per grid point from which the mean x, y and z coordinate of each point was calculated. Measurements were obtained from both Matlab and Python

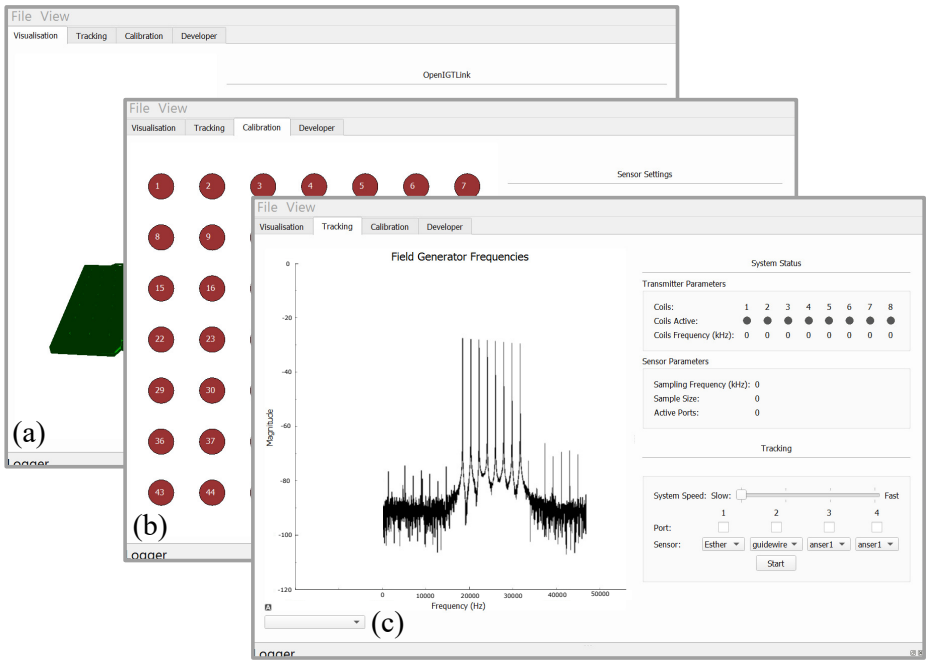

Fig. 6 Python EMT framework integrated as a graphical user interface application for Anser EMT. (a) The primary visualisation screen where instrument positions are displayed and OpenIGTLink connections can be made. (b) The calibration wizard which allows the user to calibrate a tracked instrument for use with the system by taking a sampling of 49 magnetic measurements [19]. (c) The primary interface the field generator frequencies can be set and tracked instruments may be connected and tested for use with the system.

Table 1 Performance measurements using Matlab on Windows.

Matlab	Frame size	Acq. Latency (ms)	Max. Static (Hz)	Max. Dynamic (Hz)
-	250	2.5	72	64
-	500	5	70	61
-	1000	10	65	62
-	2000	20	50	50
-	5000	50	20	20

Table 2 Performance measurements using Python framework (Windows/Linux).

Python	Frame size	Acq. Latency (ms)	Max. Static (Hz)	Max. Dynamic (Hz)
-	250	2.5/5000+*	138/120	84/70
-	500	5/2000+	142/115	95/83
-	1000	10/1000+	102/80	66/62
-	2000	20/100	51/45	52/45
-	5000	50/50	20/21	20/20

* Due to operating system driver, see discussion.

implementations. Maximum, minimum and root-mean-square (RMS) errors were calculated between the two obtained point grids. The grid obtained using the Matlab implementation was used as the reference since its performance has already been characterised in [11]. Maximum and minimum grid errors were measured as 3.1mm and 0.1mm respectively with an RMS error of 0.9mm with a standard deviation of 0.75mm.

4 Tracked needle liver ablation

The proposed framework was tested in a pre-clinical setting in IHU Strasbourg using clinically approved EM tracked needles. A preliminary feasibility study was conducted to validate electromagnetic tracking in deep-seated liver targets for radiofrequency ablation. This work shows that open-source tracking systems are capable of continuous needle tip tracking, and in this study provide visualisation in 3D environments to assist access and obscure lesions within the liver.

4.1 Experimental setup

Pre-clinical tests were performed in Institute for Image Guided Surgery in Strasbourg. The experimental setup consisted of four main components:

EM tracking The Anser EMT system was used for tracking needles during the procedure. The python framework described in section 3 was used to retrieve position data of the tracked needles and relayed to the visualisation tool via OpenIGTlink.

Visualisation The CustusX navigation platform [12] was used as the primary visualisation software during the procedure. Segmentation of the liver and identification of tumours was performed using ITK-Snap [25].

EM tracked needles The Veran Always-On Tip tracked Bx Needle (Veran Medical, St. Louis, MO) was used as targeting instruments during the procedure. Each needle kit consists of a 19 gauge needle with an EM tracked stylet in situ. The stylet contains a 5-DoF tracking sensor that is compatible with the Anser tracking system. In this study each stylet was used in conjunction with a larger 11 gauge needle (Cook Medical, Limerick, Ireland) for performing percutaneous access to the liver.

RF ablation Radiofrequency ablation (RFA) was performed using a Medtronic Cool-Tip Ablation System (Medtronic, Dublin, Ireland) and features 17 gauge electrodes.

4.2 Procedure protocol

A 34 kg female swine model was used for preclinical investigations. 8 radiopaque fiducial markers were applied to the animal's skin at bony protrusions around the liver. Percutaneous injection of a proprietary *biotumour* model was achieved at four deep-seated locations in the right lobe of the liver using an 11 gauge needle under ultrasonic guidance (Siemens Acuson S3000). Abdominal CT (Siemens Somatom Definition AS) using a soft tissue reconstruction filter (120 kV and 273 mA tube parameters and 1 mm slice thickness with 0.7 mm overlap and 512×512 resolution) was used to visualise the liver. ITK-Snap was used to segment the liver surface, vessels, rib cage and tumour models from the preoperative CT scan.

Concurrently, the tracked Veran needle stylets were calibrated for use with the Anser system by taking a sample of 49 magnetic field measurements at pre-defined positions above the system field generator [19]. Following calibration, the field generator was placed underneath the abdomen of the swine model such that the liver was located central above the field generator. An OpenIGTLink network connection was then instantiated with resulting needle position data sent to the CustusX platform. Patient-image registration was then performed in CustusX by placing the tracked stylets at the 8 radiopaque landmark sites.

Following surface registration to the skin fiducials, percutaneous cannula introduction with visualisation in the CustusX was performed by an expert user with EM tracking provided by the 19 gauge Veran tracked stylet inserted through the 11 gauge Murphy cannula. The needle was subject to movement due to respiration and the virtual needle was aimed to coincide with the virtual target on inhalation. The CustusX visualisation platform allowed for tool-tip extension for trajectory planning/prediction and real-time distance-to-target display. Once targeting was complete, the tracking stylet was replaced with a fitted RF electrode probe. RFA was applied to each target for 3 minutes using standard hepatic protocols before the electrode was removed (see Fig. 8). A postoperative CT and necropsy were performed to analyse targeting and ablation accuracy.

4.3 Results

A total of four tumour models, M1-M4, were placed in the swine model's liver. Due to leakage of the biotumour material, only models M2 and M3 produced feasible tumour-like structures for targeting. Models M1 and M4 experienced leakage during placement and were not targeted as a result. Targeted tumours, T1 and T2, were both located in the right posterior lobe and were each targeted from two different angles and trajectories. The average targeting time from point of the tracked needle insertion to removal was 3.44 minutes (range, 2 to 5.49 minutes). RFA was applied to each target for 3 minutes at a temperature of 55 °C. A single puncture was used in all cases. The mean size of targets was 1.58×0.89 cm (see Table 1). The closest distance of separation between the needle and T2 was 1.12 cm, 1.11 cm, 0 cm and was verified using postoperative CT where $\{x, y, z\}$ are referenced to the CT global imaging frame (see Table 3). Necropsy indicated two ablations within 5mm of tumours T1 and T2 (see Fig. 8). Errors are considered primarily due to breathing as needle deformation due to the 11 gauge cannula are thought to be insignificant.

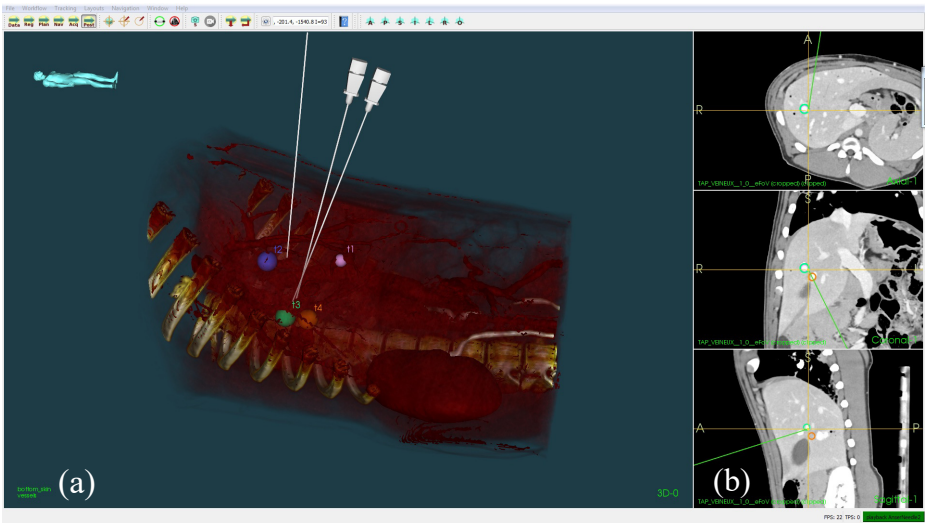

Fig. 7 CustusX visualisation of the Veran EM tracked needles during tumour targeting. The centroids of the tumours were targeted and are visualised using coloured markers.

Table 3 Locations and characteristics of the tumours placed within the liver. 2-dimensional size measurements were acquired from the axial CT view.

Tumour ID	Size [$x \times y$ cm]	Position	Liver segment
M1	1.36×0.82	Anterior right	S8
M2 (T1)	1.04×1.04	Posterior right	S7
M3 (T2)	2.12×0.73	Posterior right	S6
M4	0.65×0.74	Posterior right	S7

Table 4 Summary of targeting results. Virtual distance refers to the absolute measured distance between the needle tip and the centre of the tumour as would be measured using the visualisation in Fig. 7(a). Minimum and maximum measurements were recorded to account for motion due to breathing. Actual distance measurement were recorded in the post-operative CT scan reference frame as shown in Fig. 8(c).

Target	Virtual dist. [Min. - Max. cm]	Actual dist. [$x/y/z$ cm]	Time [mins]
T2	0.61 - 1.28	1.29/1.11/0	5.49
T2	0.45 - 1.10	1.12/1.10/0	2.00
T1	1.85 - 2.67	3.22/2.88/3.31	3.23

5 Discussion

The proposed framework was successfully integrated with Anser EMT, although the results vary greatly depending on the configured settings. Table 2 shows how performance of the Anser EMT system varies with acquisition sample size over Windows and Linux operating systems. Benchmark results on Windows are clearly favourable to Linux particularly at low sample sizes. The high latencies in Linux were found to be caused by a low-level buffer issue caused by software limitations in the NI-DAQmx Base driver for the Linux kernel. Event-based acquisition is not

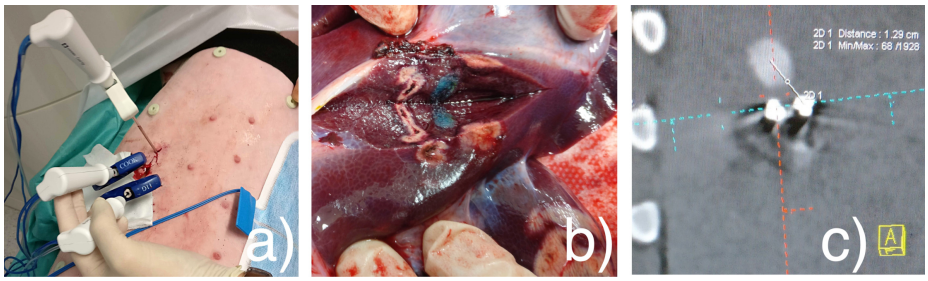

Fig. 8 (a) The swine model with percutaneous insertion of RF ablation probes. (b) Post operative necropsy showing the proximity of the ablated liver tissue (pink) and tumour model (blue). (c) Post operative CT scan showing the distance between the targeting needles and tumour model.

supported in the driver which resulted in position update latencies if the solver does not process samples at a sufficient rate. Artificially setting the acquisition time to be greater than the solving time prevents this latency issue occurring, as the solver is forced to wait until new data is available. Empirically setting the acquisition frame to 2000 (i.e. a frame acquisition time of 20 ms) mitigates the issue, although this limits the maximum effective position update rate. It can also be seen that the update speeds vary significantly depending on the movement speed of the sensor. This is due to the previous sensor position being used as the initial condition for the solver during each position update. A moving sensor causes previous sensor positions to lie further from the current true sensor position, resulting in the solver requiring more iterations to converge to the global minimum. Artificially forcing periodicity by limiting the update rate of the system prevents this issue from occurring. This approach must be implemented with care in order to avoid increasing the overall system latency.

The purpose of the accuracy benchmark is to showcase any significant differences between the two EMT software implementations. The benchmark is limited since it uses the Matlab implementation results as the reference standard, since no gold standard was available for the experiment. The reported mean error value of 0.9mm falls within the mean error value of the Matlab implementation of 1.14mm [11]. From this we can conclude that the Python implementation is of similar accuracy to the original implementation. Characterisation of this system according to the Hummel protocol [26,27] is necessary in order to fully validate the accuracy of the system under the new framework.

Applying the framework to targeted liver ablation highlighted a number of advantages of using an open approach. The study showed that 3rd party EM tracked needles can be calibrated for use with the Anser EMT for 5-DoF position and orientation tracking. This demonstrates how such a tracking framework may be used to develop and test novel 5-DoF enabled instrument designs in the pre-clinical setting. Position errors encountered during the study were caused primarily by the breathing motion of the animal model, resulting in dynamic registration error. The resulting deviations in needle targeting accuracy between inhalation and exhalation phases result in the targeting errors on the orders of centimetres shown in Table 4 which is clearly visible in Fig. 8(b). Methods of reducing these motion induced errors have been well addressed using breathing motion gating

via electromagnetic [28] and optical [29] strategies, of which this paper does not implement. However, this paper does show how an open-source tracking system can be effectively integrated into the pre-clinical setting. By providing in-depth control over the system parameters (update rates, transmission frequencies, physical models), such a system may offer advantages when developing future devices and techniques for motion compensation in tracked liver procedures.

6 Conclusion

The paper presents an open-source software framework for electromagnetic tracking systems. The framework was applied to a previously characterised tracking system with performance results recorded for different operating system environments. The framework was successfully applied and is capable of tracking needles in radiofrequency ablation therapy of the liver. Compatibility with common medical imaging visualisation tools was confirmed through communication with the CustusX visualisation platform. It is hoped that this work will assist in the translation of new electromagnetic tracking platforms, devices and instruments from research into the clinical setting.

Acknowledgements This work was support by by Science Foundation Ireland technical innovation and development award number 17/TIDA/4897. The authors would like to acknowledge the support of IHU Strasbourg surgical platform.

Compliance with ethical standards

Conflict of interest The authors declare that they have no conflict of interest.

Ethical approval Animal studies were performed at the Institute for Image Guided Surgery (IHU), Strasbourg, France. All applicable international, national, and/or institutional guidelines for the care and use of animals were followed. All procedures performed in studies involving animals were in accordance with the ethical standards of the institution at which the studies were conducted.

References

1. Alfred Michael Franz, Alexander Seitel, Nasrin Bopp, Christian Erbelding, Dominique Cheray, Stefan Delorme, Frank Grünwald, Hüdayi Korkusuz, and Lena Maier-Hein. First clinical use of the EchoTrack guidance approach for radiofrequency ablation of thyroid gland nodules. *Int. J. Comput. Assist. Radiol. Surg.*, 12(6):931–940, 2017.
2. Iwan Paolucci, Marius Schwalbe, Gian Andrea Prevost, Anja Lachenmayer, Daniel Candinas, Stefan Weber, and Pascale Tinguely. Design and implementation of a dynamic navigation technique for laparoscopic ablation of liver tumors based on electromagnetic tracked ultrasound. *Surg. Endosc.*, 32(7):3410–3419, 2018.
3. Andras Lasso, Tamas Heffter, Adam Rankin, Csaba Pinter, Tamas Ungi, and Gabor Fichtinger. PLUS: Open-source toolkit for ultrasound-guided intervention systems. *IEEE Trans. Biomed. Eng.*, 61(10):2527–2537, 2014.
4. Junichi Tokuda, Gregory S. Fischer, Xenophon Papademetris, Ziv Yaniv, Luis Ibanez, Patrick Cheng, Haiying Liu, Jack Blevins, Jumpei Arata, Alexandra J. Golby, Tina Kapur, Steve Pieper, Everette C. Burdette, Gabor Fichtinger, Clare M. Tempany, and Nobuhiko Hata. OpenIGTLink: An open network protocol for image-guided therapy environment. *Int. J. Med. Robot. Comput. Assist. Surg.*, 5(4):423–434, 2009.
5. Andinet Enquobahrie, Patrick Cheng, Kevin Gary, Luis Ibanez, David Gobbi, Frank Lindseth, Ziv Yaniv, Stephen Aylward, Julien Jomier, and Kevin Cleary. The Image-Guided Surgery Toolkit IGSTK: An open source C++ software toolkit. *J. Digit. Imaging*, 20(SUPPL. 1):21–33, 2007.

6. Baoxian Liu, Guangliang Huang, Chunlin Jiang, Ming Xu, Bowen Zhuang, Manxia Lin, Wenshuo Tian, Xiaohua Xie, Ming Kuang, and Xiaoyan Xie. Ultrasound-Guided Percutaneous Radiofrequency Ablation of Liver Metastasis From Ovarian Cancer: A Single-Center Initial Experience. *International journal of gynecological cancer : official journal of the International Gynecological Cancer Society*, 27(6):1261–1267, jul 2017.
7. C. Kunte, V. Letulé, J. Gehl, K. Dahlstroem, P. Curatolo, R. Rotunno, T. Muir, A. Occhini, G. Bertino, B. Powell, W. Saxinger, G. Lechner, S. H. Liew, R. Pritchard-Jones, P. Rutkowski, M. Zdzienicki, D. Mowatt, A. J. Sykes, A. Orlando, G. Mitsala, C. R. Rossi, L. Campana, M. Brizio, F. de Terlizzi, P. Quaglino, and J. Odili. Electrochemotherapy in the treatment of metastatic malignant melanoma: a prospective cohort study by InspECT. *British Journal of Dermatology*, 176(6):1475–1485, 2017.
8. Jin Woong Kim, Sang Soo Shin, Suk Hee Heo, Jun Hyung Hong, Hyo Soon Lim, Hyun Ju Seon, Young Hoe Hur, Chang Hwan Park, Yong Yeon Jeong, and Heoung Keun Kang. Ultrasound-guided percutaneous radiofrequency ablation of liver tumors: How we do it safely and completely. *Korean Journal of Radiology*, 16(6):1226–1239, 2015.
9. Kyoung Doo Song, Min Woo Lee, Hyunchul Rhim, Tae Wook Kang, Dong Ik Cha, Dong Hyun Sinn, and Hyo Keun Lim. Percutaneous US/MRI Fusionguided Radiofrequency Ablation for Recurrent Subcentimeter Hepatocellular Carcinoma: Technical Feasibility and Therapeutic Outcomes. *Radiology*, 288(3):878–886, 2018.
10. Akiko Tomonari, Kunihiko Tsuji, Hajime Yamazaki, Hironori Aoki, Jong Hon Kang, Yoshihisa Kodama, Yasuo Sakurai, and Hiroyuki Maguchi. Feasibility of the virtual needle tracking system for percutaneous radiofrequency ablation of hepatocellular carcinoma. *Hepatology Research*, 43(12):1352–1355, 2013.
11. Herman Alexander Jaeger, Alfred Michael Franz, Kilian O'Donoghue, Alexander Seitel, Fabian Trauzettel, Lena Maier-Hein, and Pádraig Cantillon-Murphy. Anser EMT: the first open-source electromagnetic tracking platform for image-guided interventions. *Int. J. Comput. Assist. Radiol. Surg.*, 12(6):1059–1067, 2017.
12. Christian Askeland, Ole Vegard Solberg, Janne Beate Lervik Bakeng, Ingerid Reinertsen, Geir Arne Tangen, Erlend Fagertun Hofstad, Daniel Høyer Iversen, Cecilie Våpenstad, Tormod Selbekk, Thomas Langø, Toril A Nagelhus Hernes, Håkon Olav Leira, Geirmund Unsgård, and Frank Lindseth. CustusX: an open-source research platform for image-guided therapy. *Int. J. Comput. Assist. Radiol. Surg.*, 11(4):505–519, 2016.
13. D. C. Rife and G. A. Vincent. Use of the Discrete Fourier Transform in the Measurement of Frequencies and Levels of Tones. *Bell System Technical Journal*, 49(2):197–228, 1970.
14. Helena Geirinhas Ramos and P Silva Girão. Measurement of low level DC magnetic fields using a synchronous demodulation technique. *IEEE transactions on instrumentation and measurement*, 42(2):544–546, 1993.
15. Henrik V. Sorensen and C. Sidney Burrus. Efficient Computation of the DFT with Only a Subset of Input or Output Points. *IEEE Transactions on Signal Processing*, 41(3):1184–1200, 1993.
16. Mengfei Li, Tomasz Bien, and Georg Rose. FPGA based electromagnetic tracking system for fast catheter navigation. *Int. J. Sci. Eng. Res.*, 4(9), 2013.
17. Anton Plotkin, Oren Shafrir, Eugene Paperno, and Daniel M. Kaplan. Magnetic eye tracking: A new approach employing a planar transmitter. *IEEE Trans. Biomed. Eng.*, 57(5):1209–1215, 2010.
18. Mengfei Li, Christian Hansen, and Georg Rose. A simulator for advanced analysis of a 5-DOF EM tracking systems in use for image-guided surgery. *Int. J. Comput. Assist. Radiol. Surg.*, 12(12):2217–2229, 2017.
19. Kilian O'Donoghue, David Eustace, James Griffiths, Michael O'Shea, Timothy Power, Hilary Mansfield, and Padraig Cantillon-Murphy. Catheter position tracking system using planar magnetics and closed loop current control. *IEEE Trans. Magn.*, 50(7):1–9, 2014.
20. Anton Plotkin, Eugene Paperno, Gennady Vasserman, and Ronen Segev. Magnetic tracking of eye motion in small, fast-moving animals. *IEEE Trans. Magn.*, 44(11):4492–4495, 2008.
21. K. Levenberg. A Method for the Solution of Certain Non-Linear Problems in Least Squares. *Q. Appl. Math.*, 2:164–168, 1944.
22. Pierre Cladé. PyDAQmx : a Python interface to the National Instruments DAQmx driver, 2018.
23. Travis E. Oliphant. Python for scientific computing. *Comput. Sci. Eng.*, 9(3):10–20, 2007.
24. Daniel Hiversen. PyIGTLink: A Python implementation of OpenIGTLink. 2016.
25. Paul A. Yushkevich, Joseph Piven, Heather Cody Hazlett, Rachel Gimpel Smith, Sean Ho, James C. Gee, and Guido Gerig. User-guided 3D active contour segmentation of anatomical

structures: Significantly improved efficiency and reliability. *Neuroimage*, 31(3):1116–1128, 2006.
26. J. Hummel, M. Figl, W. Birkfellner, M. R. Bax, R. Shahidi, C. R. Maurer, and H. Bergmann. Evaluation of a new electromagnetic tracking system using a standardized assessment protocol. *Phys. Med. Biol.*, 51(10):N205–N210, 2006.
27. Alfred M. Franz, Tamas Haidegger, Wolfgang Birkfellner, Kevin Cleary, Terry M. Peters, and Lena Maier-Hein. Electromagnetic tracking in medicine -A review of technology, validation, and applications. *IEEE Trans. Med. Imaging*, 33(8):1702–1725, 2014.
28. Hui Zhang, Filip Banovac, Ralph Lin, Neil Glossop, Bradford Wood, David Lindisch, Elliot Levy, and Kevin Cleary. Electromagnetic tracking for abdominal interventions in computer aided surgery. *Computer Aided Surgery*, 11(3):127–136, 2006.
29. Qinyong Lin, Rongqian Yang, Ken Cai, Peifeng Guan, Weihu Xiao, and Xiaoming Wu. Strategy for accurate liver intervention by an optical tracking system. *Biomedical Optics Express*, 6(9):3287, 2015.